International Journal of Smart Grid and Clean Energy

Comparative Stability Analysis of a Combined DFIG-based and PMSG-based Offshore Wind Farm Connected to a Large Power Grid through a LCC-HVDC Link and an HVAC Line

Li Wang*, Mi Sa-Nguyen Thi

Department of Electrical Engineering, National Cheng Kung University, Tainan City 70101, Taiwan

Abstract

This paper presents the comparative dynamic-stability analysis of an integration of a doubly-fed induction generator (DFIG)-based offshore wind farm (OWF) and a permanent-magnet synchronous generator (PMSG)-based OWF fed to a large power grid through a high-voltage AC (HVAC) line and a high-voltage direct-current (HVDC) link based on line-commutated converter (LCC). The operating performance of the studied 60-MW PMSG-based OWF is simulated by an equivalent PMSG driven by an equivalent wind turbine (WT) while an equivalent DFIG driven by an equivalent WT through an equivalent gearbox is used to simulate the operating characteristics of the 80-MW DFIG-based OWF. A frequency-domain approach based on a linearized system model using eigenvalue technique and a time-domain scheme based on a nonlinear system model subject to various disturbance conditions are both utilized to compare the damping characteristics contributed by the HVAC line and the proposed LCC-HVDC control scheme. It can be concluded from the simulation results that the proposed LCC-HVDC link is capable of rendering better damping characteristics to stabilize the studied integrated two OWFs fed to power grid subject to a severe fault than the HVAC line.

Keywords: Offshore wind farm, permanent-magnet synchronous generator, doubly-fed induction generator, high-voltage direct-current link, high-voltage AC line, dynamic stability.

1. Introduction

The utilization of high-capacity wind turbine generators (WTGs) with power rating over 5 MW for offshore wind farms (OWFs) has become a new way to meet economic benefits and high-power generation. However, an OWF with high installation-capacity sends power to onshore power grids has to face several practical challenges such as high power fluctuations, reduction of power quality, connection of weak power grids, change in operating modes of conventional power plants, etc. To solve these obstacles, a high-voltage direct-current (HVDC) link can be used to integrate several high-capacity OWFs due to its high-power control ability and fast-modulation characteristics. An HVDC link can also deliver large power over long-distance DC cables to reduce excessive voltage drop between sending end and receiving end when comparing with traditional long-distance HVAC cables with larger line-reactance voltage drop.

The analyzed outcomes of a 200-MW OWF using 25 voltage-source converters (VSCs) [1] and a 200-MW OWF using 25 current-source inverters (CSIs) [2] fed to a power grid through a multi-terminal HVDC link were discussed and compared. The simulation results of employing an AC system of 150 kV, an AC system of 400 kV, and a VSC-HVDC link for connecting three OWFs with different capacities (100 MW, 200 MW, and 500 MW) to an onshore power grid were compared [3]. An OWF using a LCC-

* Manuscript received July 10, 2012; revised August 19, 2012.
Corresponding author. Tel.: +886-6-2757575 ext. 62361; fax: +886-6-2763883; *E-mail address*: liwang@mail.ncku.edu.tw.

HVDC link fed to an onshore power network was studied in [4]. The integration of DFIG-based OWFs with a common collection bus controlled by a static synchronous compensator (STATCOM) fed to an onshore power grid through a LCC-HVDC link was investigated in [5]. Power flow control results of an OWF connected with a LCC-HVDC link through modulating the rectifier firing angle or the DC-link current were shown in [6]. The simulation outcomes and ride-through capability of a VSC-HVDC industrial system subject to voltage disturbances were demonstrated in [7]. Three different frequency controllers and their associated effects on voltage-disturbance ride-through capability of a VSC-HVDC industrial system were compared in [8]. Large power converters consisting of two series-connected 12-pulse groups and a new power converter control scheme applicable to a multilevel HVDC system were described in [9]. A STATCOM and a VSC-HVDC system used to solve operational problems in power systems were presented in [10]. The operational performance of a wind farm consisting of several IG-based WTGs and modeled by an equivalent IG incorporated VSC-HVDC system was depicted in [11]. The characteristics of a VSC-HVDC link, an HVAC cable interconnection, and a synchronous generator under a faulted condition were compared in [12], and the analyzed outcomes showed that the VSC-HVDC link was capable of offering fault ride-through capability for the studied wind farm comprising IG-based WTGs. The requirements of a DFIG-based wind farm connected to a power grid through a conventional thyristor-based HVDC link were examined in [13]. The characteristics of an IG-based OWF connected to a weak AC grid were studied, and the simulation outcomes showed that the proposed HVDC link was able to supply the variable active power of the OWF to the weak grid and keep the fluctuations of AC voltages at the point of common coupling (PCC) at an acceptable level [14].

This paper is organized as below. Section 2 introduces the configuration and the employed mathematical models for the integrated DFIG-based and PMSG-based OWFs fed to an infinite bus through a LCC-HVDC link. Section 3 depicts the eigenvalue analysis of the dominant modes of the studied system under various operating conditions. Section 4 compares transient responses of the studied system under disturbance conditions. Specific important conclusions of this paper are drawn in Section 5.

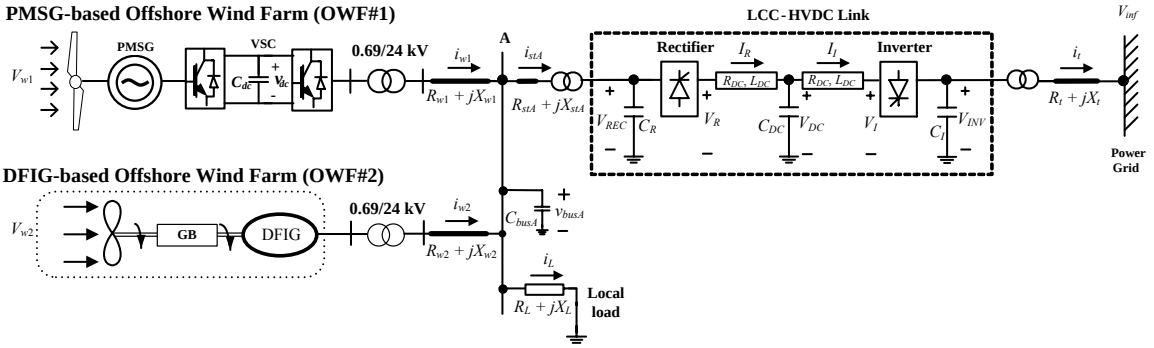

Fig. 1. Configuration of the integrated DFIG-based and PMSG-based offshore wind farms fed to an infinite bus through a LCC-HVDC link.

2. System Configuration

Fig. 1 shows the configuration of the studied system including a combined PMSG-based OWF and DFIG-based OWF is fed to a large power grid through a LCC-HVDC link. The 60-MW PMSG-based OWF (OWF#1) is represented by an equivalent aggregated variable-speed wind turbine (VSWT) driven an equivalent aggregated PMSG that is fed to bus *A* through a back-to-back power converter, a step-up transformer of 0.69/24 kV and an undersea cable. The 80-MW DFIG-based OWF (OWF#2) is represented by an equivalent aggregated VSWT with an equivalent gearbox driven an equivalent aggregated DFIG that is fed to bus *A* through a step-up transformer of 0.69/24 kV and an undersea cable. The equivalent capacitance C_{bus} is connected to the common bus *A* that is fed to an infinite bus through an offshore step-up transformer of 24/161 kV, undersea cables, the LCC-HVDC link, an onshore step-down transformer of 161/24 kV, and underground cables. The proposed 140-MW LCC-HVDC consists of a

rectifier, a T-equivalent DC cable, and an inverter, and it is used for damping improvement of the studied two OWFs subject to the power fluctuations due to wind-speed variations. The equations in the following subsections are expressed in per unit (pu) or MKS quantities except that the time variable t is in second.

2.1. Wind turbine model

The captured mechanical power by a wind turbine (WT) from wind is given by

$$P_W = \frac{1}{2}\rho A_r V_W^3 C_p(\lambda,\beta) \tag{1}$$

where P_W is the captured mechanical power (W), ρ is the air density (kg/m^3), A_r is the blade impact area (m^2), V_W is the averaged wind velocity (m/s) as depicted in [15], and C_p is the power coefficient [16] that can be expressed by

$$C_p(\psi_k,\beta) = \left[c_1\left(\frac{c_2}{\psi_k} - c_3\beta - c_4\beta^{c_5} - c_6\right)\right]\exp\left[-\frac{c_7}{\psi_k}\right] \tag{2}$$

in which

$$\frac{1}{\psi_k} = \frac{1}{\lambda + c_8\beta} - \frac{c_9}{\beta^3+1} \tag{3}$$

$$\lambda = \frac{R_{bd}\omega_{bd}}{V_W} \tag{4}$$

where λ is the tip speed ratio, β is the blade pitch angle (degrees), c_1-c_9 are constant coefficients of power coefficient C_p, ω_{bd} and R_{bd} are the blade angular velocity (rad/s) and the blade radius (m), respectively. Equation (1) is valid when the wind speed ranges between the cut-in and the rated wind speeds of the employed WT. The cut-in, rated, and cut-out wind speeds for the wind DFIG (wind PMSG) are selected as 4 (3) m/s, 14 (13) m/s, and 24 (23) m/s, respectively.

2.2. Mass-spring-damper model

Fig. 2 shows the two-inertia reduced-order equivalent mass-spring-damper model of the WT coupled to the rotor shaft of the studied wind PMSG. The model shown in Fig. 2 can also be applied to the mass-spring-damper model of the WT coupled to the rotor shaft of the studied wind DFIG through a gearbox except the employed parameters. The effect of the equivalent gearbox (GB) between the WT and the DFIG has been included in this model [17-19].

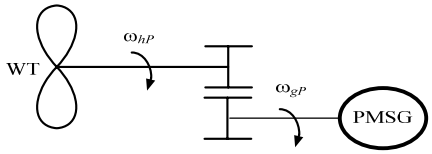

Fig. 2. Two-inertia reduced-order equivalent mass-spring-damper model of the WT coupled to the rotor shaft of the studied wind PMSG.

2.3. DFIG, PMSG models and operation of power converters

The corresponding per-unit (p.u.) q- and d-axis voltage-current equations of the DFIG and PMSG models as well as the detail operation of the converters can be referred to [20] and [21]-[22], respectively.

2.4. LCC-HVDC link model

The LCC-HVDC link model consists of an AC-to-DC converter, a DC line, and a DC-to-AC inverter [23]-[27]. The base values for the AC and DC quantities should be properly selected such that the p.u. values of DC quantities remain unchanged when they are converted to the synchronous reference frame of

the AC system [24]-[25]. The p.u. output DC voltage and current of the rectifier can be properly converted with reference to the common reference frame of the *dq*-axis of the AC system [20], [23]-[27].

Fig. 3 shows the control block diagrams of the rectifier-current regulator (RCR) of the converter and the inverter-current regulator (ICR) of the inverter [25]-[27], respectively. The p.u. equations for the RCR and the ICR can be expressed by, respectively

$$(T_R)p(\alpha_R) = K_R(I_{Rref} - I_R) - \alpha_R \quad (5)$$

$$(T_I)p(\gamma_I) = K_I(I_{Iref} - I_I) - \gamma_I \quad (6)$$

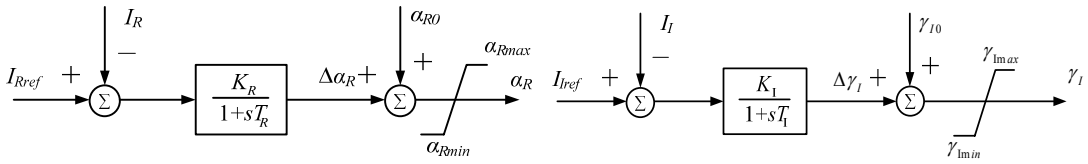

(a) (b)

Fig. 3. Block diagram of (a) the rectifier-current regulator (RCR) (b) the inverter-current regulator (ICR) of the inverter.

Table 1. Eigenvalues (rad/s) of the studied OWFs fed to an infinite bus through an HVDC link and an HVAC line under wind speed of 12 m/s for both OWFs

No.	Sub System	System with a LCC-HVDC Link	System with an HVAC Line
$\Lambda_{1\text{-}2}$		$-15.079 \pm j3.372\times10^6$	$-15.079 \pm j3.372\times10^6$
$\Lambda_{3\text{-}4}$		$-15.575 \pm j3.3919\times10^6$	$-15.571 \pm j3.3919\times10^6$
$\Lambda_{5\text{-}6}$		$-6.0411 \pm j1513.7$	$-6.0444 \pm j1548.4$
Λ_7	PMSG-based	-102.33	-102.45
Λ_8	OWF	-100.74	-100.79
Λ_9	System	-99.324	-99.297
Λ_{10}		-97.652	-97.661
$\Lambda_{11\text{-}12}$		$-0.10757 \pm j26.317$	$-0.1047 \pm j26.308$
Λ_{13}		-16.483	-16.508
Λ_{14}		-0.10428	-0.11715
$\Lambda_{15\text{-}16}$		$-4.0536 \pm j37381$	$-4.0535 \pm j37383$
$\Lambda_{17\text{-}18}$		$-4.0766 \pm j36629$	$-4.0766 \pm j36629$
$\Lambda_{19\text{-}20}$		$-6.4054 \pm j375.67$	$-48.145 \pm j450.82$
$\Lambda_{21\text{-}22}$		$-39.324 \pm j266.59$	$-6.3377 \pm j375.73$
$\Lambda_{23\text{-}24}$		$-32.691 \pm j219.51$	$-29.08 \pm j278.52$
$\Lambda_{25\text{-}26}$	DFIG-based	$-51.752 \pm j80.262$	$-51.326 \pm j75.347$
Λ_{27}	OWF	-139.76	-140.03
Λ_{28}	System	-84.385	-84.267
Λ_{29}		-104	-105.29
Λ_{30}		-10.402	-10.522
Λ_{31}		-0.43637	-0.40851
Λ_{32}		-0.029853	-0.02006
$\Lambda_{33\text{-}34}$		$-1.413 \pm j6.2201$	$-1.3401 \pm j6.2308$
$\Lambda_{35\text{-}36}$		$-9.7286 \pm j0.59184$	$-9.9696 \pm j0.32207$
$\Lambda_{37\text{-}38}$	LCC-HVDC	$-696.9 \pm j10500$	$-24.225 \pm j1566.4$
$\Lambda_{39\text{-}40}$	Link	$-270.27 \pm j8272.6$	$-35.856 \pm j1301.8$
$\Lambda_{41\text{-}42}$	or	$-604.12 \pm j5457.9$	$-26.277 \pm j1013.9$
$\Lambda_{43\text{-}44}$	HVAC Line	$-559.05 \pm j1899.1$	
Λ_{45}		-221.19	
Λ_{46}		-10.005	
Λ_{47}		-9.4153	
$\Lambda_{48\text{-}49}$	Local Load	$-562.27 \pm j4.5077$	$-521.29 \pm j22.232$

3. Eigenvalue Analysis

Table 1 lists the comparative eigenvalues of the studied two OWFs fed to a power grid through the proposed LCC-HVDC link and an HVAC line under V_W (wind speed of two OWFs) of 12 m/s. The length of the HVAC line is properly selected to have the same as the one of the LCC-HVDC link. It can be clearly seen from the results listed in Table 1 that eigenvalues eigenvalues Λ_1-Λ_{14} are the modes of the PMSG-based OWF, eigenvalues Λ_{15}-Λ_{36} are the modes of the DFIG-based OWF, eigenvalues Λ_{37}-Λ_{47} are

the modes of the proposed LCC-HVDC link or an HVAC line, and eigenvalues Λ_{48}-Λ_{49} are the modes of the local load.

When we compare the eigenvalues listed in Table 1, it is found that the employed LCC-HVDC link or HVAC line has no significant effects on the eigenvalues of the PMSG-based OWF or the local load but it has very small effects on the eigenvalues of the DFIG-based OWF. It is due to the facts that the stator windings of the equivalent wind DFIG is directly connected to the common AC bus *A* through a 0.69/24 kV step-up transformer but the wind PMSG is connected to the common AC bus *A* through a 0.69/24 kV step-up transformer and a full back-to-back power converter. The employed back-to-back power converter has the ability to decouple the effect of the PMSG and the AC system.

It is also noted that the eigenvalues of the HVAC line are three complex-conjugated modes while the eigenvalues of the LCC-HVDC consist of four complex-conjugated modes and three real modes. The four complex-conjugated modes of the LCC-HVDC system are far from the imaginary axis of the complex plane and, hence, they are quite stable and have no obvious effects on the stability of the system.

4. Analysis of Transient Responses

Fig. 4 shows the comparative transient responses of the studied system subject to a three-phase short-circuit fault at the infinite bus. The fault is suddenly applied to the system at t = 5.0 s and lasts for 0.1 s. The blue lines and the the red lines shown in Fig. 4 are the transient responses of the studied system with the HVAC line and with the LCC-HVDC link, respectively.

It can be observed from the transient responses of the active power, the rotational speed, and the terminal voltage of the PMSG-based OWF respectively shown in Figs. 4(a)-4(c) that the proposed LCC-HVDC link can offer better damping characteristics to the quantities of the PMSG-based OWF than the HVAC line. The transient responses of the active power, the rotational speed, and the terminal voltage of the DFIG-based OWF respectively shown in Figs. 4(d)-4(f) have sharp peaks at t = 5.0 s when the system with the proposed HVAC line but the proposed LCC-HVDC link can effectively suppress the sharp peaks at the time of applied fault and the quantities of the DFIG-based OWF can quickly return back to the steady-state values.

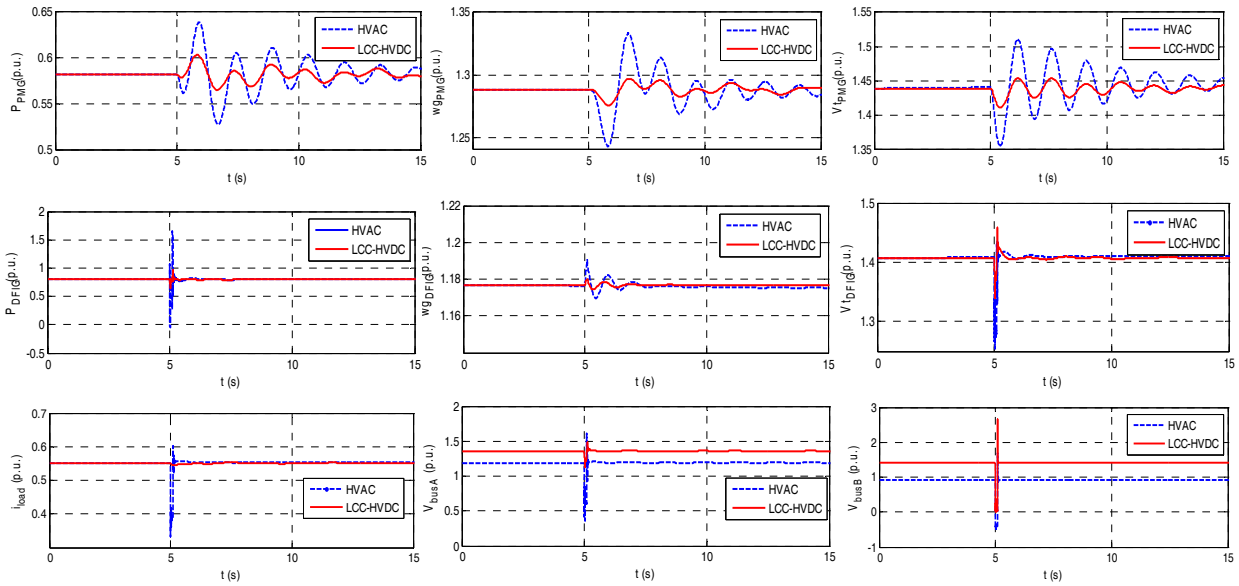

Fig. 4. Comparative transient responses of the studied system subject to a three-phase short-circuit fault at the infinite bus:(a) P_{PMSG}; (b) ω_{PMSG}; (c) v_{PMSG}; (d) P_{DFIG}; (e) ω_{DFIG}; (f) v_{DFIG}; (g) i_{load}; (h) v_{busA}; (i) v_{busB}

The transient response of the load current, the voltage of bus *A*, and the voltage of bus *B* respectively shown in Figs. 4(g)-4(i) demonstrate that the LCC-HVDC link can have smaller variations on the load

current and the voltages of buses *A* and *B* than the HVAC line. It can be concluded from the transient simulation responses shown in Fig. 4 that the studied system with the proposed LCC-HVDC link has the ability to suppress large variations on the quantities of the system due to the applied severe fault at the infinite bus.

5. Conclusion

This paper has presented the comparative stability analysis of an integration of a DFIG-based OWF and a PMSG-based OWF fed to a power grid through a LCC-HVDC link and an HVAC line. The eigenvalue technique has been employed to show the comparative damping characteristics contributed by the HVAC line and the proposed LCC-HVDC link. Transient responses of the studied system subject to a severe three-phase short-circuit fault at the power grid have demonstrated the proposed LCC-HVDC link can effectively suppress large variations on the quantities of the studied system.

Acknowledgements

The authors would like to thank the financial support from National Science of Council (NSC) of Taiwan under Grant NSC 101-ET-E-006-005-ET, Grant NSC 101-3113-P-006-014, and Grant NSC-101-3113-E-006-013

References

[1] Jovcic D. Interconnecting offshore wind farms using multiterminal VSC-based HVDC. In: *Proc. of IEEE Power Engineering Society*, 2006:1–7.

[2] Jovcic D, Milanovic J. Offshore wind farm based on variable frequency mini-grids with multiterminal DC interconnection.. In: *Proc. of the 8th IEE International conference on AC-DC Transmission (ACDC)*, 2006: 215–219.

[3] Bresesti P, Kling WL, Hendriks RL, Vailati R. HVDC connection of offshore wind farms to the transmission system. *IEEE Transactions on Energy Conversion*, 2007; 22(1):137–143.

[4] Bozhko SV, Giménez RB, Li R, Clare JC, Asher GM. Control of offshore DFIG-based wind farm grid with line-commutated HVDC connection. *IEEE Transactions Energy Conversion*, 2007; 22(1):171–78.

[5] Bozhko S, Asher G, Li R, Clare J, Yao L. Large offshore DFIG-based wind farm with line-commutated HVDC connection to the main grid: Engineering studies. *IEEE Transactions Energy Conversion*, 2008; 23(1):1119–127.

[6] Li R, Bozhko S, Asher G. Frequency control design for offshore wind farm grid with LCC-HVDC link connection. *IEEE Transactions Power Electronics*, 2008; 23(3):31085–1092.

[7] Du C, Agneholm E, Olsson G. Use of VSC-HVDC for industrial systems having onsite generation with frequency control. *IEEE Transactions Power Delivery*, 2008; 23(4):42233–2240.

[8] Du C, Agneholm E, Olsson G. Comparison of different frequency controllers for a VSC-HVDC supplied system. *IEEE Transactions Power Delivery*, 2008; 23(4):42224–2232.

[9] Murray NJ, Arrillaga J, Liu YH, Watson NR. Flexible reactive power control in multigroup current-sourced HVDC interconnections. *IEEE Transactions Power Delivery*, 2008; 23(4):42160–2167.

[10] Jaén A, Acha E, Gómez Expósito A. Voltage source converter modeling forpower system state estimation: STATCOM and VSC-HVDC. *IEEE Transactions Power Systems*, 2008; 23(1):41552–1559.

[11] Yin M, Li G, Zhou M, Liu Y. Analysis and control of wind farm incorporated VSC-HVDC in unbalanced conditions. In: *Proc. IEEE/PES Transaction and Distribution Conference*, 2005:1–6.

[12] Reidy A, Watson R. Comparison of VSC based HVDC and HVAC interconnections to a large offshore wind farm. In: *Proc. IEEE Power Engineering Society General Meeting*, 2005:1–8.

[13] Xiang D, Ran L, Bumby JR, Tavner PJ, Yang S. Coordinated control of an HVDC link and doubly fed induction generators in a large offshore wind farm. *IEEE Transactions Power Delivery*, 2006; 21(1):1463–470.

[14] Koutiva XI, Vrionis TD, Vovos NA, Giannakopoulos GB. Optimal integration of an offshore wind farm to a weak AC grid. *IEEE Transactions Power Delivery*, 2006; 21(2):2987–994.

[15] Anderson PM, Bose A. Stability simulation of wind turbine system. *IEEE Transactions Power Apparatus and Systems*, 1983; 102(12):123791–3795.

[16] Heier S, Waddington R. *Grid Integration of Wind Energy Conversion Systems*. New York: John Wiley & Sons; 1998.

[17] Trudnowski DJ, Gentile A, Khan JM, Petritz EM. Fixed-speed wind-generator and wind-park modeling for transient stability studies. *IEEE Transactions Power Systems*, 2004; 19(4):41911-1917.

[18] Muyeen SM, et al. Transient stability analysis of wind generator system with the consideration of multi-mass shaft model. In: *Proc.of International Conference on Power Electronics and Drives Systems*, 2006:511–516.
[19] Cartwright P, Holdsworth L, Ekanayake JB, Jenkins N. Coordinated voltage control strategy for a doubly-fed induction generator (DFIG)-based wind farm. In: *Proc. IEE Gener. Transm. Distrib*, 2004:495–502.
[20] Wang L, Wang KH. Dynamic stability analysis of a DFIG-based offshore wind farm connected to a power grid through an HVDC link. *IEEE Transactions Power Systems*, 2011; 26(3):31501-1510.
[21] Wang L and Li CN. Dynamic stability analysis of a tidal power generation system connected to an onshore distribution system. *IEEE Transactions on Energy Conversion*, 2011; 26(4):41191–1197.
[22] Wang L and Liu JH. Dynamic analysis of a grid-connected marine-current power generation system connected to a distribution system. *IEEE Transactions Power Systems*, 2010; 25(4):41798-1805.
[23] Peterson HA, Krause PC. A direct-and quadrature-axis representation of a parallel AC and DC power system.. *IEEE Transactions Power App. Systems*, 1966; 86(3):3210–224.
[24] Rahim AHMA, El-Amin IM. Stabilization of a high voltage AC/DC power system, I. Evaluation of control strategies. *IEEE Transactions Power Systems*, 1986; 1(11):11128–136.
[25] Hsu YY, Wang L. Damping of a parallel ac-dc power system using PID power system stabilizers and rectifier current regulators. *IEEE Transactions Energy Conversion*, 1988; 3(3):4540–549.
[26] Wang L. A comparative study of damping schemes on damping generator oscillations. *IEEE Transactions Power Systems*, 1993; 8(2):613–619.
[27] Hsu YY, Wang L. Modal control design of an HV DC system for the damping of subsynchronous oscillations. *IEE Proceedings Generation, Transmission and Distribution, Part C*, 1989; 136(2):276–286.